Energy Storage Materials 23 (2019) 8–16

Contents lists available at ScienceDirect

Energy Storage Materials

journal homepage: www.elsevier.com/locate/ensm

Non-flammable electrolyte for dendrite-free sodium-sulfur battery

Junxiong Wu [a], Jiapeng Liu [a], Ziheng Lu [a,e], Kui Lin [c,d], Yu-Qi Lyu [a], Baohua Li [c], Francesco Ciucci [a,b,*], Jang-Kyo Kim [a,**]

[a] Department of Mechanical and Aerospace Engineering, The Hong Kong University of Science and Technology, Clear Water Bay, Kowloon, Hong Kong, China
[b] Department of Chemical and Biological Engineering, The Hong Kong University of Science and Technology, Clear Water Bay, Hong Kong, China
[c] Graduate School at Shenzhen, Tsinghua University, Shenzhen 518055, China
[d] School of Materials Science and Engineering, Tsinghua University, Beijing 100084, China
[e] Shenzhen Institutes of Advanced Technology, Chinese Academy of Sciences, Shenzhen 518055, China

ARTICLE INFO

Keywords:
Room-temperature sodium-sulfur battery
Nonflammable electrolyte
Fluoroethylene carbonate
Trimethyl phosphate

ABSTRACT

Room temperature (RT) sodium-sulfur (Na-S) batteries are a promising technology for stationary energy storage thanks to their high energy density of 1274 Wh kg^{-1} and low cost. However, RT Na-S batteries are hazardous because they use highly volatile and flammable electrolytes. Here, we develop a new nonflammable electrolyte for RT Na-S batteries, consisting of sodium trifluoromethanesulfonimide (NaTFSI) in a mixture of trimethyl phosphate (TMP) and fluoroethylene carbonate (FEC). The nonflammable electrolyte facilitates highly stable and reversible Na plating/stripping during cycles. The dendrite-free Na-S battery with the NaTFSI/TMP+FEC electrolyte delivers a remarkable reversible capacity of 788 mAh g^{-1} after 300 cycles at 1C, corresponding to a negligible capacity decay below 0.04% per cycle. The *ab initio* molecular dynamics simulations and surface analysis reveal the formation of a NaF-rich solid electrolyte interphase (SEI) film with reduced interfacial resistance thanks to the introduction of FEC into the electrolyte. The formed NaF SEI layer suppresses the growth of Na dendrites on the anode, enhancing the electrochemical performance of the RT Na-S batteries. The new findings reported here will shed new light on dendrite-free RT Na-S batteries by the rational design of nonflammable electrolytes.

1. Introduction

Conventional high-temperature (HT) sodium-sulfur (Na-S) batteries have been used for grid-scale storage applications because of their excellent lifespan, low cost, and the abundance of raw materials [1–5]. However, these Na-S batteries typically operate at above 300 °C to ensure fast diffusion of Na^+ ions in the solid electrolyte [1–3,6]. At these temperatures, both S and Na electrodes are in a molten state, leading to a series of technological challenges with reference to safety, material cost, and HT sealing [6]. To resolve these challenges, room temperature (RT) Na-S batteries have been developed [2–5]. Unfortunately, RT Na-S batteries are hazardous: (1) conventional organic electrolytes are highly volatile and flammable with tangible fire and explosion risks under abusive conditions, such as impact, overheating, and overcharging [7–9]; (2) because of the growth of Na dendrites [4–6]. Nonflammable, electrochemically stable, and cost-effective electrolytes are needed to address the above issue. Several nonflammable electrolytes have recently been explored including ionic liquids and inorganic solid-state electrolytes [6,10–12]. However, the former electrolytes are expensive, while the latter suffer from higher electrode/electrolyte interfacial resistances than liquid-based electrolytes [11–13].

In search of nonflammable electrolytes for RT Na-S batteries, organic phosphates have been explored because of their low viscosity, wide range of useable temperature, ability to dissolve high Na salt concentrations, and intrinsic nonflammability [7,14]. Among various phosphate solvents, trimethyl phosphate (TMP) is particularly promising because of its low viscosity (2.3 mPa s), high dielectric constant (21.6), and wide temperature range of its liquid phase (between −46 and 197 °C) [7,8,15,16]. However, TMP decomposes on carbonaceous and Na metal anodes, and cannot form stable solid electrolyte interphase (SEI) films on the anode surface [7,17,18]. Therefore, ternary mixed additives have been incorporated to improve the stability of TMP on graphite anodes in Li-ion

* Corresponding author. Department of Mechanical and Aerospace Engineering, The Hong Kong University of Science and Technology, Clear Water Bay, Kowloon, Hong Kong, China.
** Corresponding author.
E-mail addresses: francesco.ciucci@ust.hk (F. Ciucci), mejkkim@ust.hk (J.-K. Kim).

https://doi.org/10.1016/j.ensm.2019.05.045
Received 16 February 2019; Received in revised form 27 May 2019; Accepted 29 May 2019
Available online 1 June 2019

batteries [18]. Recently, a concentrated electrolyte with 3.3 M NaN($SO_2F)_2$ in TMP was used to achieve the stable charge and discharge of hard carbon for more than 1000 cycles in Na-ion batteries [8]. However, nonflammable electrolytes have not been reported for RT Na-S batteries delivering high capacities and stable cyclability.

Sulfurized polyacrylonitrile (SPAN), firstly developed by the Yang's group, has attracted great interest as a cathode material for lithium-sulfur (Li-S) batteries because no polysulfide dissolution occurred in the redox process of SPAN [13,19–21]. Therefore, batteries with a SPAN cathode have shown excellent cyclic performances [13,20,21]. In addition, the fabrication of the SPAN composite is simple and can be easily scaled-up. In light of these reasons, we selected SPAN as the cathode material for our RT Na-S battery.

In this study, we developed a nonflammable electrolyte, 2 M NaTFSI/TMP+FEC. This electrolyte displayed a high ionic conductivity of about 6.0 mS cm^{-1} and facilitated the stable Na plating/stripping cycles on the Na metal anodes of RT Na-S batteries. The X-ray photoelectron spectroscopy (XPS) and *ab initio* molecular dynamics simulations demonstrated the formation of a mechanically strong sodium fluoride (NaF)-rich SEI film promoted by the newly developed electrolyte. The NaF-rich SEI film suppressed the growth of Na dendrites on the anode, which in turn ameliorated the performance of the RT Na-S batteries to deliver a remarkable capacity of 788 mAh g^{-1} after 300 cycles at 1C with a capacity retention of about 90%. In brief, our nonflammable electrolyte significantly improved the safety of RT Na-S batteries without compromising the electrochemical performance.

2. Experimental section

2.1. Preparation of SPAN cathodes

An isopropyl alcohol (Aladdin, 99.5%) slurry of PAN (Aldrich, Mw 150000) and S (Aldrich, AR 99.5%) in a weight ratio of 1:8 was homogeneously mixed using a ball miller (Tencan XQM-0.4A) at 500 rpm for 6 h. Then, the slurry was dried in a vacuum oven at 50 °C for 6 h to evaporate the solvent. Finally, the SPAN composite was obtained by heating the power in a tube furnace at 300 °C for 450 min under N_2 (purity>99.99%) flow. As a control, PAN without sulfur was heat-treated at 300 °C and the product is denoted as pPAN.

2.2. Preparation of electrolytes

NaTFSI (DoDoChem, 99.8%), Sodium hexafluorophosphate ($NaPF_6$ Sigma-Aldrich, 98%), and sodium perchlorate ($NaClO_4$, Sigma-Aldrich, 98%) were dried in a vacuum oven at 100 °C for 12 h. TMP (Sigma-Aldrich, 99%), ethyl carbonate (EC, Sigma-Aldrich, 99%), and diethyl carbonate (DEC, Sigma-Aldrich, 99%) were dehydrated by 4 Å molecular sieves. FEC (Aladdin, >98%) was used as received. The electrolytes were prepared by dissolving the specific salts into the solvents inside a glove box (Mikrounda, <0.01 ppm of oxygen and <0.01 ppm of moisture) filled with Ar. The 2 M NaTFSI/TMP+FEC electrolyte was obtained by dissolving 2 M NaTFSI salt into the mixture of TMP/FEC (in a volume ratio, v/v = 7:3), where "M" stands for molar concentration. The water content in the electrolytes was determined by Karl-Fisher titration. The values for the 2 M NaTFSI/TMP+FEC and 2 M NaTFSI/TMP electrolytes are approximately 9.5 ppm and 9.2 ppm, respectively.

2.3. Characterization

X-ray diffraction (XRD) was carried out using a Philips PW1830 diffractometer with Cu Kα radiation at a scanning rate of 5°min^{-1}. The morphology and structure of materials were examined on a field emission scanning electron microscope (FE-SEM, HITACH 8010U) and a transmission electron microscope (TEM, JEOL 2010). The Raman spectra were collected using a Raman spectroscometer (HORIBA Labram HR Evolution) equipped with a 532 nm Ar-ion laser. Fourier transformed infrared (FTIR) spectra were taken using a Bruker Vertex 70 spectrometer. XPS was carried out using a PHI 5000 VersaProbe II with a monochromatic Al Kα X-ray source (1486.6 eV) at 25 W and 5 kV with a beam spot size of 100 μm. Depth profile measurements were obtained by sputtering the Na using an Ar^+ ion gun at 2 kV. The S content in the SPAN composite was determined by elemental analyzer (vario Micro cube). The ionic conductivities of the electrolytes were measured by the electrochemical impedance spectra taken from 1 Hz to 100 kHz at a current amplitude of 5 mV on an electrochemical workstation (VSP-300, Bio-Logic) at RT. The test cells were assembled by soaking two stainless steel blocking electrodes in the electrolyte. For the *ex situ* SEM characterization, the Na anodes were rinsed with dimethyl carbonate (DMC) inside the glove box and transferred into the SEM using a vacuum chamber.

2.4. Electrochemical measurements

We prepared the electrodes by mixing the SPAN composite, carbon black and carboxymethyl cellulose in a weight ratio of 8:1:1 in deionized (DI) water to form a homogeneous slurry. The slurry was coated onto a thin aluminum foil, which was dried in a vacuum oven at 60 °C for 12 h. The SPAN electrodes were punched into circular discs with a diameter of 12 mm. The CR2032-type Na/SPAN coin cells were assembled in the Ar-filled glove box with SPAN, Na metal foil, and glass microfiber (Whatman, GF/D) as the cathode, anode, and separator, respectively. The electrolyte/S volume-to-mass ratio is around 100 mL g^{-1}. The cyclic performance and rate tests were recorded using a Land 2001A battery testing system over a voltage range from 0.8 to 3 V at RT. The capacities were normalized with respect to sulfur loading in the SPAN composite whose mass loading varied between 1.2 and 1.5 mg cm^{-2}. The cyclic voltammetry (CV) measurements were performed between 0.8 and 3 V and electrochemical impedance spectroscopy (EIS) was conducted in a frequency range from 0.01 Hz to 100 kHz on a VSP-300 electrochemical workstation. The electrochemical stability of the electrolyte was studied via linear sweep voltammetry (LSV) and CV. A stainless-steel (SS) blocking electrode was employed as the working electrode while a Na foil was used as both the counter and reference electrode. The LSV curves were recorded from open circuit voltage up to 6.0 V versus Na/Na^+ at a scanning rate of 1 mV s^{-1}. An identical blocking configuration was used for the CV measurements, where the voltage range was selected from −1 to 5 V versus Na/Na^+ and the scanning rate was set at 5 mV s^{-1}. We also assembled Na/Na symmetric cells, where the Na foil had a diameter of 12 mm.

2.5. Computational methods

The lowest unoccupied molecular orbital (LUMO) energies of FEC and TMP were calculated using the Gaussian 09 software [22]. We first optimized the structures of FEC and TMP molecules, using the density functional theory (DFT) with the B3LYP exchange–correlation functional [23,24] and the 6–31++G (d, p) basis set. The vibrational frequency was calculated to confirm the true minimum structures on the potential energy surface. The LUMO energies of molecules were calculated based on the optimized structure.

We also calculated the LUMO energies of FEC and TMP using Vienna *ab initio* simulation package (VASP) with the general gradient approximation (GGA) and the Perdew-Burke-Ernzerhof (PBE) functional [25,26]. We obtained virtually identical values within 0.01 eV. Consequently, *ab initio* molecular dynamics (AIMD) simulations were carried out using VASP. The model was constructed using six TMP molecules and four FEC molecules in a volume ratio of TMP to FEC being 7:3 on a three-layer 4×2 supercell of Na (110) surface. For the "pure" TMP system, ten TMP molecules were used. A 15 Å vacuum layer was added to limit the image-image interactions. The cutoff kinetic energy and the energy convergence criterion were set at 400 eV and 10^{-4} eV, respectively. The AIMD simulations were performed in 10 ps with a time step of 1.0 fs in the NVT ensemble at 300 K with the Nosé thermostat [27–30].

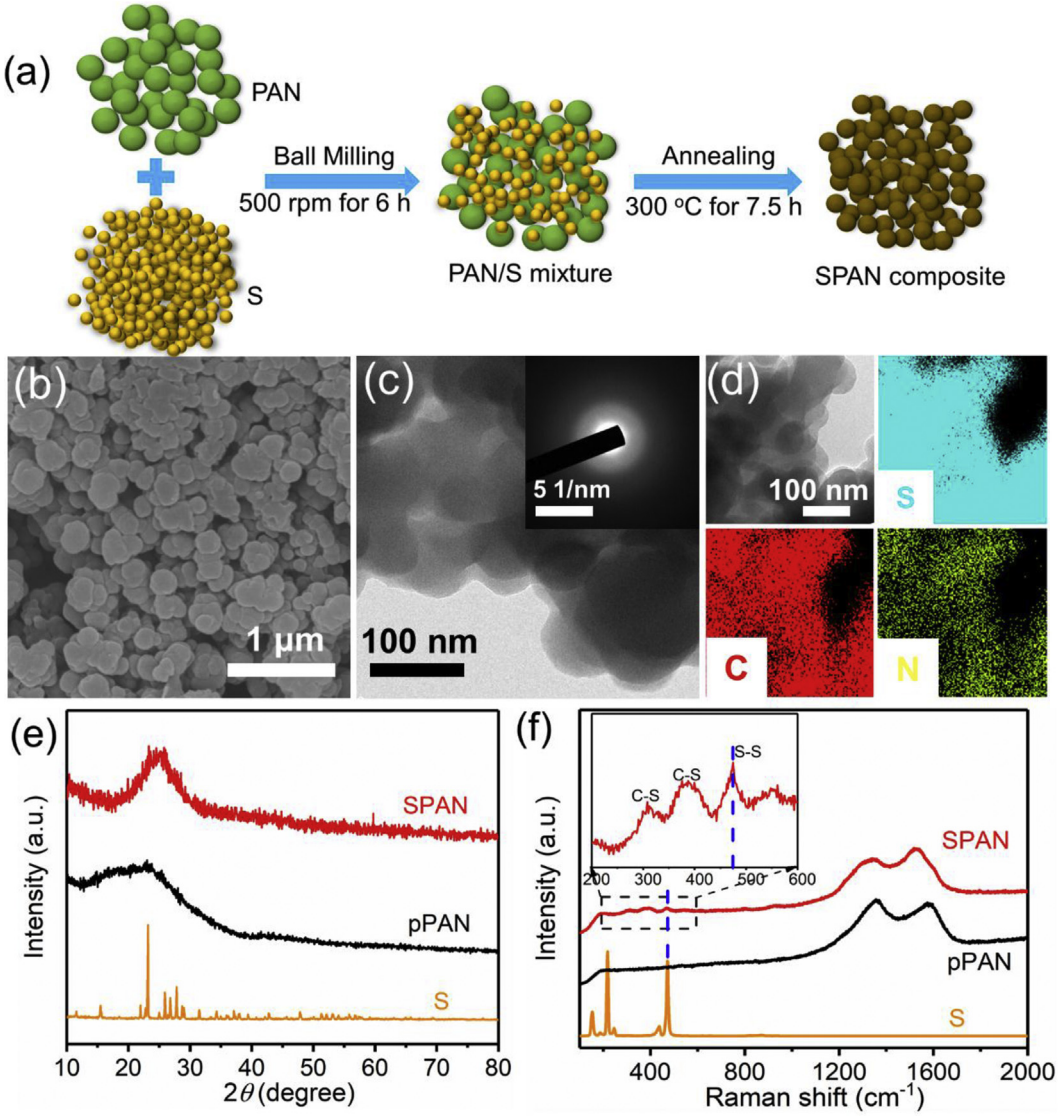

Fig. 1. (a) Schematic illustration of the synthesis procedure, (b) SEM, (c) TEM and SAED pattern (inset of c), (d) TEM-EDS images of the SPAN composite. (e) XRD patterns, and (f) Raman spectra of the SPAN composite, pPAN, and S.

3. Results and discussion

The fabrication process of SPAN composite is schematically shown in Fig. 1a. The SEM image shown in Fig. 1b indicates that the average particle size of SPAN was ~100 nm, a value further confirmed by TEM (Fig. 1c). High-resolution TEM images (Fig. S1) and the selected area electron diffraction (SAED) patterns (see inset of Fig. 1c) both indicate that SPAN has an amorphous structure. The EDS elemental maps suggest that C, S, and N were homogeneously distributed in SPAN (Fig. 1d). According to the elemental analysis, S constituted ~43 wt% of the mass of the SPAN composite (Table S1). The XRD patterns of the pPAN, S, and SPAN are presented in Fig. 1e. The XRD pattern of SPAN has a broad peak centered at ~25°, corresponding to the hexahydric-ring layer of pyrolyzed PAN, which is analogous to disordered carbon [21,31]. No crystalline S_8 peaks were detected in the SPAN, suggesting that the S in SPAN was amorphous. The Raman spectrum of elemental S has three distinct peaks at 153, 218, and 473 cm^{-1} [21], whereas the SPAN exhibited three peaks with much weaker intensities, as shown in Fig. 1f. The two peaks centered at 308 and 384 cm^{-1} can be assigned to the C-S bonds formed by the reaction between S and PAN during heating [21,32], whereas the peak at 474 cm^{-1} can be attributed to the presence of S-S bonds [31]. The FTIR spectra further confirmed the presence of C-S and S-S bonds in SPAN composite (Fig. S2). The peaks in the region from 1200 to 1600 cm^{-1} and the peak at 803 cm^{-1} suggest the formation of six-membered rings containing C=C and C=N bonds. Besides, the peaks at 515, 668, and 938 cm^{-1} can be attributed to S-S stretching, C-S stretching, and ring breath of the side-chain containing S-S bonds, respectively [20,21].

Fig. 2a and b compare the interactions of the carbonate electrolyte (2 M NaTFSI/EC+DEC (1:1, v/v)) and 2 M NaTFSI/TMP+FEC electrolyte with a direct flame. The carbonate electrolyte burned quickly and continuously even after removing the exogenous fire (Fig. 2a), while the TMP-based electrolyte could not be ignited (Fig. 2b). When dropping the carbonate electrolyte over a flame, the flame was intensified (Movie S1). In contrast, the 2 M NaTFSI/TMP+FEC electrolyte was an effective fire extinguisher (Movie S2). This occurred because TMP scavenges the active hydrogen radicals to delay the combustion chain reaction [13,33].

Supplementary data related to this article can be found at https://doi.org/10.1016/j.ensm.2019.05.045.

The ionic conductivities of the NaTFSI/TMP+FEC electrolytes with different salt concentrations are shown in Fig. 2c. The 2 M NaTFSI/TMP+FEC electrolyte had the highest conductivity (6.0 mS cm^{-1}) among the three measured. The electrochemical stability of the 2 M NaTFSI/TMP+FEC and 2 M NaTFSI/TMP electrolytes against Na metal was

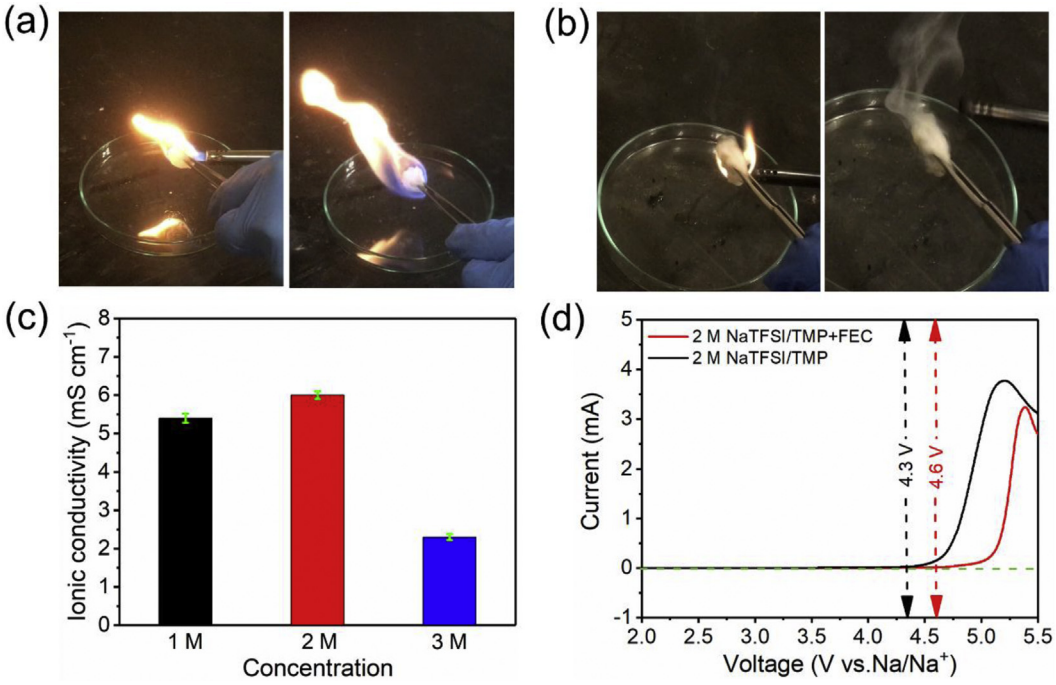

Fig. 2. Combustion tests of (a) 2 M NaTFSI/EC+DEC (1:1, v/v) and (b) 2 M NaTFSI/TMP+FEC electrolytes. (c) RT ionic conductivities of the electrolytes with different salt concentrations. (d) Electrochemical stability window of 2 M NaTFSI/TMP+FEC and 2 M NaTFSI/TMP electrolytes determined by LSV at a scan rate of 1 mV s^{-1} with a SS foil as the working electrode and a Na foil as the reference and counter electrode.

measured by LSV and CV. The LSV curves shown in Fig. 2d suggest that the 2 M NaTFSI/TMP+FEC electrolyte possesses an electrochemical window of about 4.6 V, which is larger than that of the 2 M NaTFSI/TMP without FEC (4.3 V). The CV scans were carried out from −1 to 5 V vs. Na/Na^+ at a scan rate of 5 mV s^{-1}. As shown in Fig. S3, two oxidation/reduction peaks corresponding to Na plating/stripping on SS appeared at around 0 V vs. Na/Na^+ [7]. The CV curve of Na/2 M NaTFSI/TMP+FEC/SS cell presents comparable oxidation/reduction peaks, suggesting good reversibility of the Na plating/stripping process. In contrast, the area of the reduction peak is much larger than that of the oxidation peak using 2 M NaTFSI/TMP. This discrepancy may be attributed to side reactions taking place during the Na plating process. The CV profiles of the RT Na/SPAN batteries were also recorded with the 2 M NaTFSI/TMP+FEC electrolyte. As shown in Fig. S4, the reduction and oxidation scans nearly overlapped from the 3rd cycle onwards, supporting the high reversibility of the Na/SPAN batteries.

We also explored the impact of salt concentration on rate performance of the Na/SPAN cells, see Fig. S5. Among the cells studied, the one with the 2 M NaTFSI/TMP+FEC electrolyte showed the best overall performance. The reversible capacity obtained for the battery with the 3 M NaTFSI/TMP+FEC electrolyte was even worse than the one recorded with the 1 M counterpart, consistently with much lower ionic conductivity, see Fig. 2c. Furthermore, electrolytes with FEC concentrations ranging 0 to 50 vol% were also tested. As shown in Fig. S6, the electrolyte containing 30 vol% FEC yielded the best capacity (821 mAh g^{-1} after 100 cycles) among the four studied. Therefore, we used the 30 vol% FEC in all ensuing electrochemical tests. The impact of the Na salts on the cyclic performance of Na/SPAN batteries was also investigated. As shown in Fig. S7, the capacity was more stable in the electrolyte with the NaTFSI salt compared to that of batteries that used $NaClO_4$ and $NaPF_6$ salts.

Fig. 3a compares the cyclic performance of the Na/SPAN cells with two different electrolytes with and without FEC. The cells were activated at 0.1C for 3 cycles before carrying out the cyclic tests at 0.2C (Fig. S8). The reversible capacity and the Coulombic efficiency were significantly improved by the addition of FEC. The battery containing FEC in the electrolyte delivered a reversible capacity of 1070 mAh g^{-1} after 100 cycles, a value much high than the ~150 mAh g^{-1} obtained for the cell without FEC. After the cyclic tests, the EIS was measured to evaluate the impedance parameters and Fig. 3b shows the Nyquist plots of the Na/SPAN cells in the above two electrolytes. The EIS spectra were fitted with the equivalent circuit shown in Fig. S9 and the estimated impedance parameters are given in Table S2. In the absence of FEC, the interfacial resistance (R_f) and charge transfer resistance (R_{ct}) were ~384 and ~326 Ω, respectively. These values were significantly reduced to ~228 and ~110 Ω, respectively, upon addition of FEC in the electrolyte, indicating the formation of favorable SEI layers and ameliorating the transfer of charge. Further, the presence of FEC in the electrolyte improved the rate capability of the battery, as shown in Fig. 3c. The cell with the 2 M NaTFSI/TMP+FEC electrolyte delivered remarkable reversible capacities of ~1025, 880, 750, 550, and 300 mAh g^{-1} at 0.2, 0.5, 1, 2, and 4C, respectively, along with a high capacity of 1020 mAh g^{-1} after reverting to 0.2C. The corresponding discharge/charge curves are shown in Fig. 3d. In contrast, the cell with the 2 M NaTFSI/TMP electrolyte had far lower capacities of 734, 354, 128, and 45 mAh g^{-1}, respectively.

Fig. 3e shows the long-term cyclic performance of the Na/SPAN cells with the 2 M NaTFSI/TMP+FEC electrolyte at 1C. The battery delivered a remaining capacity of 788 mAh g^{-1} after 300 cycles, corresponding to an exceptionally low capacity decay below 0.04% per cycle. In contrast, the cyclic performance of the Na/SPAN cells with the FEC-free electrolyte was typical of fast fading with a ~1% capacity decay per cycle and a remaining capacity of only ~100 mAh g^{-1} after 300 cycles. As will be discussed in detail by *ex situ* SEM and XPS analyses, the improved cyclic performance can be attributed to the formation of stable interfaces at both cathode and anode when the electrolyte containing FEC was used. The cyclic performance of the Na/SPAN cells with electrolytes containing different compositions of EC, DEC and FEC are shown in Fig. S10. The specific capacity of the Na/SPAN cell with the 2 M NaTFSI/EC+DEC (1:1, v/v) electrolyte faded quickly to 200 mAh g^{-1} after 300 cycles at 1C; the capacity decay was ~0.5%/cycle. With the same FEC (30 vol%) in the latter electrolyte, the cyclic stability of the battery was significantly improved, confirming its ameliorative effect. Table S3 compares the electrochemical performance of RT Na-S batteries reported in the

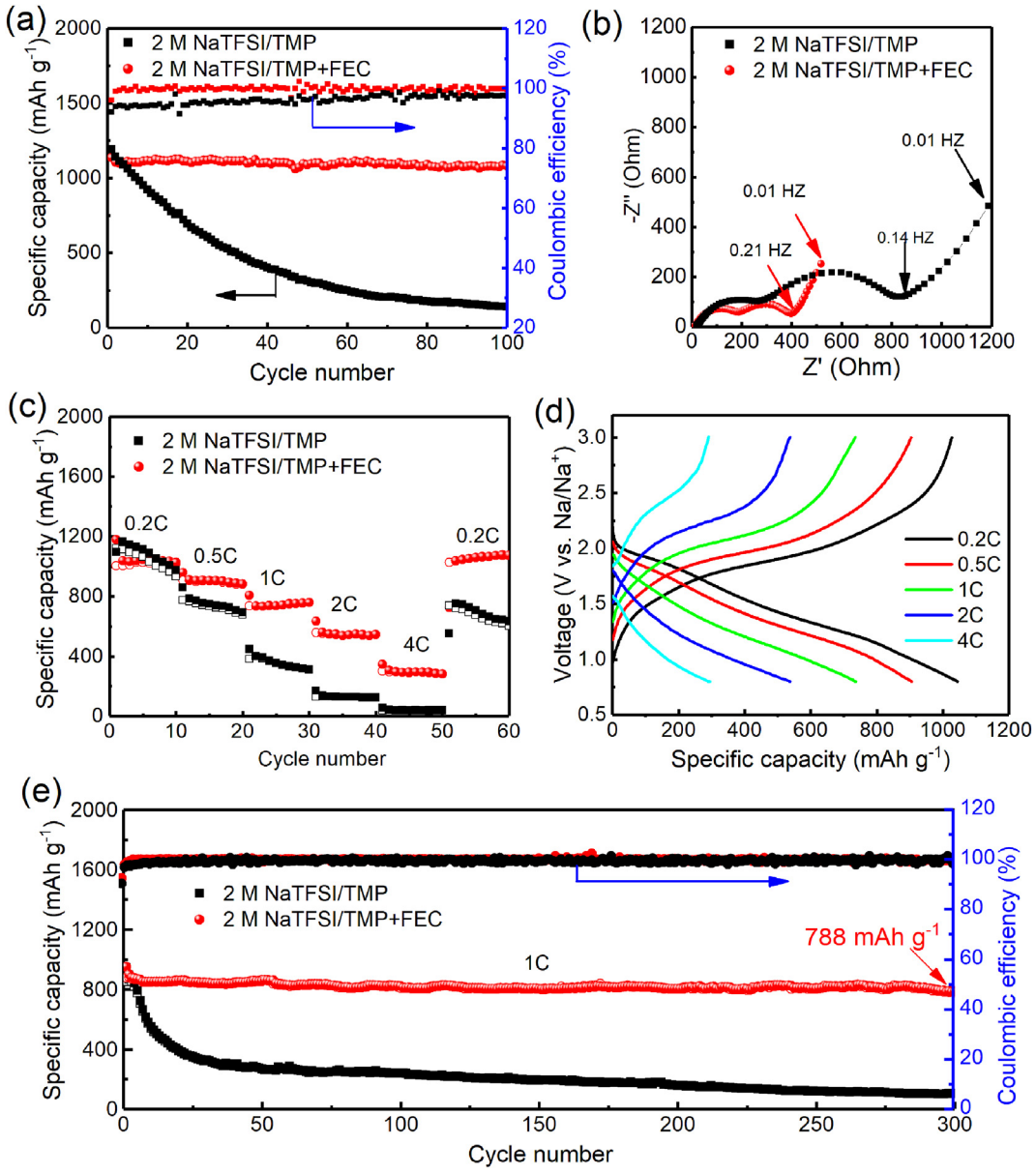

Fig. 3. Electrochemical performance of the Na/SPAN cells with the 2 M NaTFSI/TMP+FEC and 2 M NaTFSI/TMP electrolytes. (a) Cyclic performance at 0.2C; (b) Nyquist plots of the EIS spectra obtained after 100 cycles; (c) rate performance at several current densities, and (d) corresponding charge/discharge curves. (e) Cyclic performance at 1C.

literature. The current Na/SPAN cell with the 2 M NaTFSI/TMP+FEC electrolyte outperformed previous reported state-of-the-art batteries in terms of both cyclic performance and rate capability.

To evaluate the stability of Na plating/stripping with the 2 M NaTFSI/TMP+FEC electrolyte, Na|Na symmetric cells were assembled. Fig. 4a shows the voltage profiles of symmetric cells assembled using the 2 M NaTFSI/TMP+FEC and 2 M NaTFSI/TMP electrolytes at a current density of 1 mA cm^{-2}. The plating/stripping time was 0.5 h. The symmetric cell without FEC electrolyte exhibited irregular voltage fluctuations throughout the test. In contrast, the cells with the electrolyte containing FEC are characterized by a highly stable Na plating/stripping for 160 h. The voltage profiles of Na|Na symmetric cells with plating/stripping capacities of 1 mAh cm^{-2} and 3 mAh cm^{-2} are shown in Fig. S11. The symmetric cells with the FEC added to the electrolyte displayed a much stable Na plating/stripping response for 100 h. Remarkably, the Na|Na cell in the same electrolyte was able to cycle with excellent stability for 1000 h at 0.3 mA cm^{-2} (Fig. 4b). To further confirm the role of FEC in supporting stable Na plating and stripping, analogous tests were conducted in carbonate electrolytes. The voltage profiles shown in both Fig. 4a and Fig. S12 reveal that the presence of FEC in the electrolyte improved the cyclic stability of the symmetric cells. The superior cyclic stability of the symmetric cells in an electrolyte containing FEC was verified by the *ex situ* EIS measurements after 20 cycles, as shown in Fig. S13. The interfacial resistances estimated from the EIS spectra were ~805 and 1300 Ω, for the cells in the electrolytes with and without FEC, respectively. This result again confirms the improved electrode/electrolyte interface due to FEC [34,35]. Furthermore, the morphology of the Na anode surface was examined after 50 plating/stripping cycles, as shown in Fig. 4c and d. While the surface of the Na anode remained flat and dense in the 2 M NaTFSI/TMP+FEC electrolyte, mossy and dead Na can be observed when FEC is not present. The porous and loose Na may be attributed to the dead Na, which leads to a large interfacial resistance, agreeing with the EIS results [36].

Xu et al. reported that FEC can reduce the solubility of sodium polysulfides and be used to construct a robust SEI on the Na anode upon cycling [5]. For the specific SPAN cathode, the short-chain poly(sulfide)s

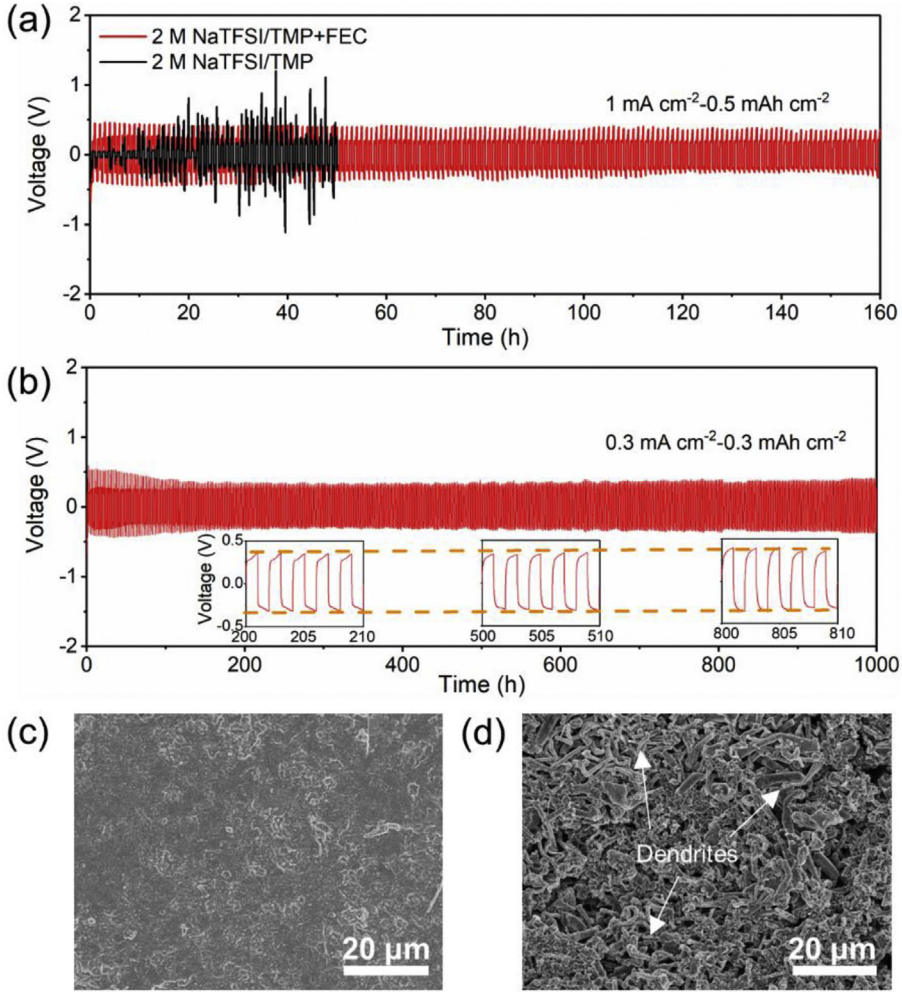

Fig. 4. Voltage profiles measured during cyclic Na plating and stripping from the Na|Na symmetric cells at current densities of (a) 1.0 and (b) 0.3 mA cm^{-2}. SEM images of Na anode surfaces after 50 plating/stripping cycles with the (c) 2 M NaTFSI/TMP+FEC and (d) 2 M NaTFSI/TMP electrolytes.

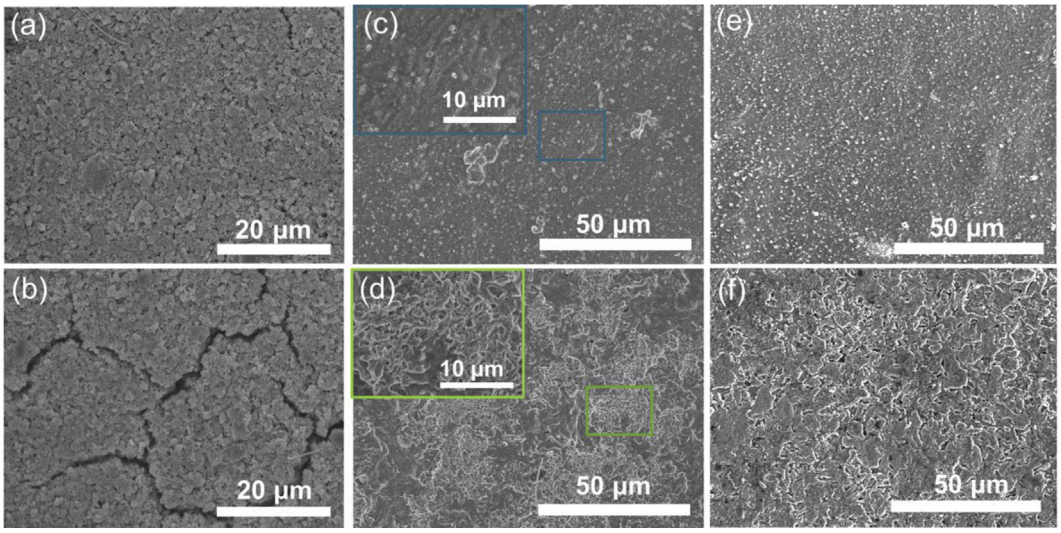

Fig. 5. SEM images of the SPAN cathode and Na anode surfaces of the Na/SPAN batteries after 100 cycles at 1C with the (a, c) 2 M NaTFSI/TMP+FEC and (b, e) 2 M NaTFSI/TMP electrolytes, respectively. SEM images of the Na anode surfaces of the Na/SPAN batteries after 100 cycles at 1C with the (e) 2 M NaTFSI/EC+DEC+FEC (3.5:3.5:3, v/v/v) and (f) 2 M NaTFSI/EC+DEC (1:1, v/v) electrolytes.

formed upon discharge have limited solubility in ester electrolyte [20, 37]. Therefore, the shuttle effect does not play an important role in Na/SPAN batteries in spite of reduced solubility of sodium polysulfides due to FEC. The morphological impact of FEC on the SPAN cathode was

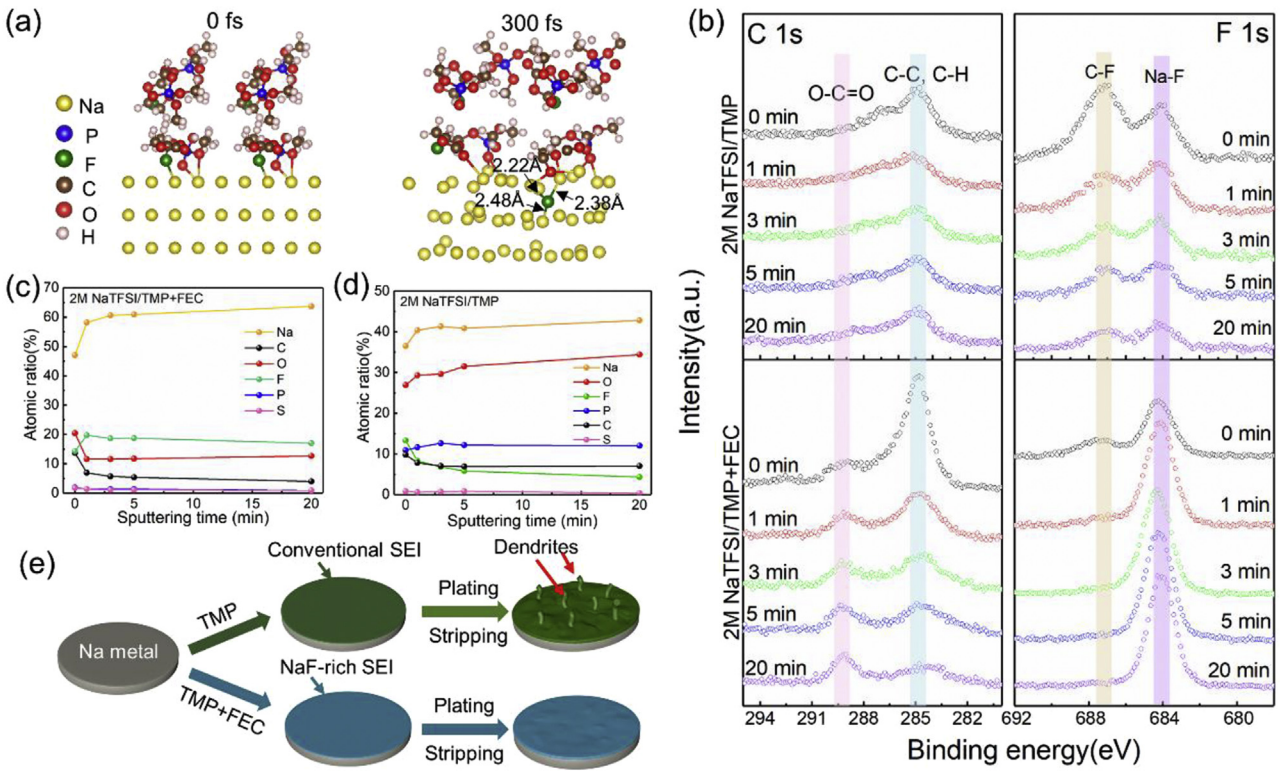

Fig. 6. (a) Snapshot of the AIMD simulation of FEC and TMP molecules on a three-layer Na (110) surface. (b) C 1s and F 1s XPS spectra of the SEI layer on the Na metal anode induced by the 2 M NaTFSI/TMP+FEC and 2 M NaTFSI/TMP electrolytes at various sputtering times. Atomic ratios of various elements as a function of sputtering time for the SEIs formed using (c) 2 M NaTFSI/TMP+FEC and (d) 2 M NaTFSI/TMP. The data were recorded after 100 cycles at 1C. (e) Schematic illustration of the impact of NaF-rich SEI on the stability of the Na electrode.

checked by disassembling the Na/SPAN cells tested in the 2 M NaTFSI/TMP+FEC and 2 M NaTFSI/TMP electrolytes for 100 cycles. As shown in Fig. 5a, The SPAN cathode tested in the electrolyte containing FEC displayed no obvious pulverization or fracture. Instead, cracks were present in the absence of FEC, see Fig. 5b. The Na deposition in the presence of FEC took place uniformly leading to an even and smooth surface (Fig. 5c). In contrast, without FEC the Na metal anode surface was far rougher (Fig. 5d). The above observations confirm that the FEC promotes the formation of stable interfaces at both cathode and Na metal anode. To confirm the role of FEC in inhibiting the growth of Na dendrites, FEC was also added to the 2 M NaTFSI/EC+DEC (1:1, v/v) electrolyte. The stability of carbonate-based electrolytes (2 M NaTFSI/EC+DEC (1:1, v/v) and 2 M NaTFSI/EC+DEC+FEC (3.5:3.5:3, v/v/v)) against the Na anode was examined by SEM (Fig. 5e and f). One should note that, if 30 vol% FEC was added to 2 M NaTFSI/EC+DEC (1:1, v/v), then the surface of the Na electrode was significantly smoother than the one without FEC even after 100 cycles.

It is well-established that FEC reduces before conventional carbonate solvents, such as EC and DEC, to form an SEI layer. This earlier reduction occurs because FEC has a lower LUMO energy compared to the conventionally used solvents [36,38]. We confirmed that FEC has a lower LUMO energy than that of TMP according to first-principles calculations, see Fig. S14. This means that FEC was easier to reduce than TMP on the surface of Na metal. Furthermore, *ab initio* molecular dynamics simulations were conducted to understand the formation of the SEI layer induced by FEC. Six TMP molecules and four FEC molecules were put on a three-layer Na (110) slab to simulate the reaction between the Na anode and the electrolyte containing both TMP and FEC, as shown in Fig. 6a. The carbon-fluorine (C-F) bond in the FEC molecule broke after only 300 fs from the start of the simulation. The calculated Na-F distance (at 300 fs), $d = 2.36 \pm 0.14$ Å, is consistent with the experimental value, $d = 2.32$ Å, of NaF crystals [39]. Following this formation, the Na-F bond was still maintained (Fig. S15). This result suggests the generation of NaF on the surface of the Na metal anode. The as-obtained NaF is considered as an important component of SEI. In contrast, as shown in Fig. S16, TMP decomposed on the surface of the Na metal.

The FEC-induced SEI layer developed on the Na anode after 100 cycles was probed by Ar^+ ion etching-assisted XPS, as shown in Fig. 6b. Regarding the C 1s spectra, the features at 284.8 eV and 289.4 eV can be assigned to C- (C, H) and O-C═O, respectively. The latter is commonly formed in FEC-containing electrolyte and is attributed to the decomposition of FEC [38,40]. The F 1s spectra obtained with and without FEC additive show distinct characteristics. We should first note that the peaks at 689.4 eV and 684.5 eV are attributable to the presence of C-F bonds in $TFSI^-$ and NaF, respectively [41–43]. The relative intensity of the NaF peak for the FEC-containing electrolyte is much higher than its FEC-free counterpart. Fig. 6 c and d show the atomic concentration of various elements as a function of etching time for the SEI formed using both the 2 M NaTFSI/TMP+FEC and the 2 M NaTFSI/TMP electrolytes. The content of F element in FEC-induced SEI can be estimated to be around 20%, which is higher than that recorded for the FEC-free electrolyte. Besides, the concentrations of P and O in the FEC-induced SEI are also much lower. In summary, the above results strongly suggest that the presence of FEC in the 2 M NaTFSI/TMP+FEC electrolyte reduces the reaction between TMP and Na metal and promotes the generation of a stable NaF-rich SEI layer. Based on the aforementioned result, Fig. 6e schematically illustrates the impact of the NaF-rich SEI on the stability and reversibility of the Na electrode. After repeating plating and stripping, mossy and dendritic Na formed if FEC was not added. In contrast, with the 2 M NaTFSI/TMP+FEC electrolyte, a conformal and robust NaF-rich SEI formed on top of the Na anode. This SEI suppressed side reactions between the electrolyte and the Na anode as well as the growth of Na dendrites [42–45]. Therefore, the NaF-rich SEI facilitated stable and reversible Na plating/stripping and promoted the long cycle life of the RT

Na/SPAN batteries.

4. Conclusions

We have developed a nonflammable electrolyte for dendrite-free RT Na-S battery. The nonflammable electrolyte, 2 M NaTFSI/TMP+FEC, has a high ionic conductivity of about 6 mS cm^{-1} and a wide electrochemical window nearing 4.6 V vs. Na/Na^{+}. The first-principle calculations revealed that FEC has a lower LUMO energy than TMP, implying that FEC is easily reduced on the surface of Na metal, leading to the formation of NaF-rich SEI films. The NaF-rich SEI layer guarantees a stable electrode/electrolyte interface and, in turn, suppresses the growth of Na dendrites. Consequently, the dendrite-free RT Na-S batteries with the 2 M NaTFSI/TMP+FEC electrolyte deliver a remarkable capacity of 788 mAh g^{-1} after 300 cycles at 1C with a capacity retention of about 90%, as well as excellent rate capabilities. This work offers an effective approach using nonflammable organic phosphate electrolytes for dendrite-free and high-safety RT Na-S batteries.

Acknowledgements

This project was financially supported by the Research Grants Council (GRF Projects: 16207615, 16227016, 16204517 and 16208718) and the Innovation and Technology Commission (ITF project ITS/001/17) of Hong Kong SAR. FC also thanks the Guangzhou Science and Technology Program (No. 2016201604030020) and the Science and Technology Planning Project of Guangdong Province, China (No. 2016A050503042). The authors also appreciate the technical assistance from the Advanced Engineering Materials facilities (AEMF) and the Materials Characterization and Preparation Facilities (MCPF) of HKUST.

Appendix A. Supplementary data

Supplementary data to this article can be found online at https://doi.org/10.1016/j.ensm.2019.05.045.

References

[1] Y.-X. Wang, B. Zhang, W. Lai, Y. Xu, S.-L. Chou, H.-K. Liu, S.-X. Dou, Room-temperature sodium-sulfur batteries: a comprehensive review on research progress and cell chemistry, Adv. Energy Mater. 7 (2017), 1602829.
[2] S. Xin, Y.X. Yin, Y.G. Guo, L.J. Wan, A high-energy room-temperature sodium-sulfur battery, Adv. Mater. 26 (2014) 1261–1265.
[3] A. Manthiram, X. Yu, Ambient temperature sodium-sulfur batteries, Small 11 (2015) 2108–2114.
[4] D. Zhou, Y. Chen, B. Li, H. Fan, F. Cheng, D. Shanmukaraj, T. Rojo, M. Armand, G. Wang, A stable quasi-solid-state sodium–sulfur battery, Angew. Chem. Int. Ed. 57 (2018) 10168–10172.
[5] X. Xu, D. Zhou, X. Qin, K. Lin, F. Kang, B. Li, D. Shanmukaraj, T. Rojo, M. Armand, G. Wang, A room-temperature sodium-sulfur battery with high capacity and stable cycling performance, Nat. Commun. 9 (2018) 3870.
[6] J. Yue, F. Han, X. Fan, X. Zhu, Z. Ma, J. Yang, C. Wang, High-performance all-inorganic solid-state sodium-sulfur battery, ACS Nano 11 (2017) 4885–4891.
[7] Z. Zeng, X. Jiang, R. Li, D. Yuan, X. Ai, H. Yang, Y. Cao, A safer sodium-ion battery based on nonflammable organic phosphate electrolyte, Adv. Sci. 3 (2016), 1600066.
[8] J. Wang, Y. Yamada, K. Sodeyama, E. Watanabe, K. Takada, Y. Tateyama, A. Yamada, Fire-extinguishing organic electrolytes for safe batteries, Nat. Energy 3 (2017) 22–29.
[9] D.H. Wong, J.L. Thelen, Y. Fu, D. Devaux, A.A. Pandya, V.S. Battaglia, N.P. Balsara, J.M. DeSimone, Nonflammable perfluoropolyether-based electrolytes for lithium batteries, Proc. Natl. Acad. Sci. 111 (2014) 3327–3331.
[10] D.R. MacFarlane, N. Tachikawa, M. Forsyth, J.M. Pringle, P.C. Howlett, G.D. Elliott, J.H. Davis, M. Watanabe, P. Simon, C.A. Angell, Energy applications of ionic liquids, Energy Environ. Sci. 7 (2014) 232–250.
[11] C. Zhao, L. Liu, X. Qi, Y. Lu, F. Wu, J. Zhao, Y. Yu, Y.S. Hu, L. Chen, Solid-state sodium batteries, Adv. Energy Mater. (2018), 1703012.
[12] A. Manthiram, X. Yu, S. Wang, Lithium battery chemistries enabled by solid-state electrolytes, Nat. Rev. Mater. 2 (2017) 16103.
[13] H. Yang, Q. Li, C. Guo, A. Naveed, J. Yang, Y. Nuli, J. Wang, Safer lithium-sulfur battery based on nonflammable electrolyte with sulfur composite cathode, Chem. Commun. 54 (2018) 4132–4135.
[14] X. Jiang, X. Liu, Z. Zeng, L. Xiao, X. Ai, H. Yang, Y. Cao, A nonflammable Na^{+}-based dual-carbon battery with low-cost, high voltage, and long cycle life, Adv. Energy Mater. 8 (2018) 802176.
[15] P. Shi, H. Zheng, X. Liang, Y. Sun, S. Cheng, C. Chen, H. Xiang, A highly concentrated phosphate-based electrolyte for high-safety rechargeable lithium batteries, Chem. Commun. 54 (2018) 4453–4456.
[16] Z. Zeng, V. Murugesan, K.S. Han, X. Jiang, Y. Cao, L. Xiao, X. Ai, H. Yang, J.-G. Zhang, M.L. Sushko, J. Liu, Non-flammable electrolytes with high salt-to-solvent ratios for Li-ion and Li-metal batteries, Nat. Energy 3 (2018) 674–681.
[17] X. Wang, E. Yasukawa, S. Kasuya, Nonflammable trimethyl phosphate solvent-containing electrolytes for lithium-ion batteries: I. The use of an amorphous carbon anode, J. Electrochem. Soc. 148 (2001) A1066–A1071.
[18] X. Wang, C. Yamada, H. Naito, G. Segami, K. Kibe, High-concentration trimethyl phosphate-based nonflammable electrolytes with improved charge–discharge performance of a graphite anode for lithium-ion cells, J. Electrochem. Soc. 153 (2006) A135–A139.
[19] W. Wang, Z. Cao, G.A. Elia, Y. Wu, W. Wahyudi, E. Abou-Hamad, A.-H. Emwas, L. Cavallo, L.-J. Li, J. Ming, Recognizing the mechanism of sulfurized polyacrylonitrile cathode materials for Li–S batteries and beyond in Al-S batteries, ACS Energy Lett. 3 (2018) 2899–2907.
[20] Z.-Q. Jin, Y.-G. Liu, W.-K. Wang, A.-B. Wang, B.-W. Hu, M. Shen, T. Gao, P.-C. Zhao, Y.-S. Yang, A new insight into the lithium storage mechanism of sulfurized polyacrylonitrile with no soluble intermediates, Energy Storage Mater. 14 (2018) 272–278.
[21] S. Wei, L. Ma, K.E. Hendrickson, Z. Tu, L.A. Archer, Metal-sulfur battery cathodes based on PAN-sulfur composites, J. Am. Chem. Soc. 137 (2015) 12143–12152.
[22] M. Frisch, G. Trucks, H.B. Schlegel, G.E. Scuseria, M.A. Robb, J.R. Cheeseman, G. Scalmani, V. Barone, B. Mennucci, G. Petersson, Gaussian 09, Revision a. 02, gaussian, Inc., Wallingford, CT 200, 2009.
[23] S.F. Boys, F. d. Bernardi, The calculation of small molecular interactions by the differences of separate total energies. Some procedures with reduced errors, Mol. Phys. 19 (1970) 553–566.
[24] C. Lee, W. Yang, R.G. Parr, Development of the colle-salvetti correlation-energy formula into a functional of the electron density, Phys. Rev. B 37 (1988) 785.
[25] G. Kresse, J. Furthmüller, Efficient iterative schemes for ab initio total-energy calculations using a plane-wave basis set, Phys. Rev. B 54 (1996) 11169.
[26] J.P. Perdew, K. Burke, M. Ernzerhof, Generalized gradient approximation made simple, Phys. Rev. Lett. 77 (1996) 3865.
[27] Z. Lu, F. Ciucci, Structural origin of the superionic na conduction in $Na_2B_{10}H_{10}$ closo-borates and enhanced conductivity by na deficiency for high performance solid electrolytes, J. Mater. Chem. A 4 (2016) 17740–17748.
[28] H. Jiang, Z. Lu, M. Wu, F. Ciucci, T. Zhao, Borophene: a promising anode material offering high specific capacity and high rate capability for lithium-ion batteries, Nano Energy 23 (2016) 97–104.
[29] Z. Lu, C. Chen, Z.M. Baiyee, X. Chen, C. Niu, F. Ciucci, Defect chemistry and lithium transport in Li_3OCl anti-perovskite superionic conductors, Phys. Chem. Chem. Phys. 17 (2015) 32547–32555.
[30] J. Wu, Z. Lu, K. Li, J. Cui, S. Yao, M. I.-u. Haq, B. Li, Q.-H. Yang, F. Kang, F. Ciucci, J.-K. Kim, Hierarchical MoS_2/carbon microspheres as long-life and high-rate anodes for sodium-ion batteries, J. Mater. Chem. A 6 (2018) 5668–5677.
[31] Y. Liu, W. Wang, J. Wang, Y. Zhang, Y. Zhu, Y. Chen, L. Fu, Y. Wu, Sulfur nanocomposite as a positive electrode material for rechargeable potassium-sulfur batteries, Chem. Commun. 54 (2018) 2288–2291.
[32] T.H. Hwang, D.S. Jung, J.S. Kim, B.G. Kim, J.W. Choi, One-dimensional carbon-sulfur composite fibers for Na-S rechargeable batteries operating at room temperature, Nano Lett. 13 (2013) 4532–4538.
[33] X. Wang, E. Yasukawa, S. Kasuya, Nonflammable trimethyl phosphate solvent-containing electrolytes for lithium-ion batteries: I. Fundamental properties, J. Electrochem. Soc. 148 (2001) A1058–A1065.
[34] Y. Zhang, W. Luo, C. Wang, Y. Li, C. Chen, J. Song, J. Dai, E.M. Hitz, S. Xu, C. Yang, High-capacity, low-tortuosity, and channel-guided lithium metal anode, Proc. Natl. Acad. Sci. 114 (2017) 3584–3589.
[35] S.S. Chi, Y. Liu, W.L. Song, L.Z. Fan, Q. Zhang, Prestoring lithium into stable 3D nickel foam host as dendrite-free lithium metal anode, Adv. Funct. Mater. 27 (2017), 1700348.
[36] X.Q. Zhang, X.B. Cheng, X. Chen, C. Yan, Q. Zhang, Fluoroethylene carbonate additives to render uniform Li deposits in lithium metal batteries, Adv. Funct. Mater. 27 (2017), 1605989.
[37] S. Warneke, M. Eusterholz, R. Zenn, A. Hintennach, R. Dinnebier, M. Buchmeiser, Differences in electrochemistry between fibrous SPAN and fibrous S/C cathodes relevant to cycle stability and capacity, J. Electrochem. Soc. 165 (2018) A6017–A6020.
[38] Z. Zhu, Y. Tang, Z. Lv, J. Wei, Y. Zhang, R. Wang, W. Zhang, H. Xia, M. Ge, X. Chen, Fluoroethylene carbonate enabling a robust LiF-rich solid electrolyte interphase to enhance the stability of the MoS_2 anode for lithium-ion storage, Angew. Chem. Int. Ed. 57 (2018) 3656–3660.
[39] R. Wyckoff, Interscience publishers, New York, New York rocksalt structure, Cryst. Struct. 1 (1963), 85-237.
[40] J. Zheng, M.H. Engelhard, D. Mei, S. Jiao, B.J. Polzin, J.-G. Zhang, W. Xu, Electrolyte additive enabled fast charging and stable cycling lithium metal batteries, Nat. Energy 2 (2017) 17012.
[41] Q. Shi, Y. Zhong, M. Wu, H. Wang, H. Wang, High-performance sodium metal anodes enabled by a bifunctional potassium salt, Angew. Chem. Int. Ed. 130 (2018) 9207–9210.

[42] L. Ji, M. Gu, Y. Shao, X. Li, M.H. Engelhard, B.W. Arey, W. Wang, Z. Nie, J. Xiao, C. Wang, J.-G. Zhang, J. Liu, Controlling SEI formation on SnSb-porous carbon nanofibers for improved Na ion storage, Adv. Mater. 26 (2014) 2901–2908.
[43] X. Fan, L. Chen, O. Borodin, X. Ji, J. Chen, S. Hou, T. Deng, J. Zheng, C. Yang, S.-C. Liou, Non-flammable electrolyte enables Li-metal batteries with aggressive cathode chemistries, Nat. Nanotechnol. 13 (2018) 715.
[44] S. Wu, Y. Qiao, K. Jiang, Y. He, S. Guo, H. Zhou, Tailoring sodium anodes for stable sodium-oxygen batteries, Adv. Funct. Mater. 28 (2018), 1706374.
[45] Z.W. Seh, J. Sun, Y. Sun, Y. Cui, A highly reversible room-temperature sodium metal anode, ACS Cent. Sci. 1 (2015) 449–455.